

# Theoretical Study of the Spontaneous Electron-Hole Exciton Condensates between n and p-type MoS<sub>2</sub> Monolayers, toward beyond CMOS Applications

Xian Wu, Xuehao Mou, Leonard F. Register, and Sanjay K. Banerjee  
 Microelectronics Research Center, The University of Texas at Austin  
 10100 Burnet Road Building 160, Austin, Texas 78758, USA  
 xianwu@utexas.edu

**Abstract**—We model equilibrium properties of possible room-temperature electron-hole exciton condensates formed between two dielectrically separated transition metal dichalcogenide (TMD) layers, MoS<sub>2</sub> layers here, toward application to novel beyond CMOS devices. Our simulation method employs an interlayer Fock exchange interaction incorporated into an otherwise intra-layer tight-binding Hamiltonian within a maximally-localized Wannier function (MLWF) basis set.

**Keywords**—MoS<sub>2</sub>; bilayer; exciton condensate; maximally-localized Wannier functions; tight-binding; Fock exchange interaction

## I. INTRODUCTION

Excitons, electron-hole pairs bound by their Coulomb interaction, can form a condensed state in semiconductors similar to that of electron-electron pairs in superconductors at low temperature, e.g., [1,2]. Exciton condensation gives rise to novel quantum transport properties including near-perfect Coulomb drag and ultralow-voltage negative differential resistance (NDR) [2-4]. Ultralow-power beyond-CMOS devices based on these properties have been proposed, e.g., the *Bilayer pseudoSpin Field-Effect Transistor* (BiSFET) [5].

So far, exciton condensates and associated transport properties have been observed experimentally at very low temperature and using magnetic fields to create partially filled (electron-like) and partially empty (hole-like) Landau levels in the subbands of adjacent III-V quantum wells [1,2]. However, for a synergy of reasons, including achievable layer proximity, identical or similarly shaped conduction and valence band structures, and a largely separately adjustable dielectric environment, two-dimensional (2D) material systems offer the opportunity for exciton condensation at higher temperatures and absent magnetic fields. With two oppositely-charged and dielectrically separated 2D layers, the condensate of the spatially indirect interlayer excitons may even survive at room temperature [6-8].

Graphene was the first host explored to accommodate the interlayer exciton condensate [6,7], and work is ongoing. However, another group of materials, the transition metal dichalcogenides (TMDs) now being explored by many, may prove a more hospitable host [8,9]. TMD materials have the form of MX<sub>2</sub>, with M being a transition metal atom (Mo, W, etc.) and X being a chalcogen atom (S, Se, etc.). These atoms

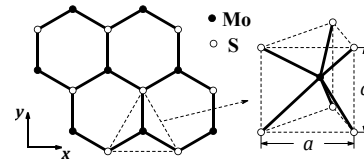


Fig. 1. Top and three-dimensional views of a MoS<sub>2</sub> monolayer crystal structure.

can form an atomically thin quasi-2D monolayer with a sheet of M atoms sandwiched by two sheets of X atoms, as for the MoS<sub>2</sub> monolayer shown in Fig. 1.

In this paper, we perform simulations on the behavior of the exciton condensate in an illustrative bilayer MoS<sub>2</sub> system as a starting point. However, in practice, staggered or even broken gap band alignments between dissimilar TMDs would be preferable to avoid the need for otherwise large interlayer and gate electric fields.

## II. SIMULATION METHOD

### A. Structure

We model a MoS<sub>2</sub> bilayer system with two perfectly aligned MoS<sub>2</sub> monolayers. The two MoS<sub>2</sub> monolayers are separated with center-to-center separation  $d$  by an interlayer dielectric. This interlayer dielectric and, more importantly, the extra-layer dielectric environment, as well as any free-carrier screening in the presence of a condensate, are simply described by a uniform effective dielectric constant  $\epsilon_r$  in this work focused on the qualitative physics.

### B. Basis set

With a tight-binding basis set  $|\mathbf{R}n\rangle$  where  $\mathbf{R}$  labels the real-space lattice sites and  $n$  labels the index of basis functions in each unit cell, the electron states in this bilayer system can be written as

$$|\psi\rangle = \sum_{\mathbf{R},n} \varphi_{\mathbf{R}n} |\mathbf{R}n\rangle = \left( \sum_{\mathbf{R},n=1}^N + \sum_{\mathbf{R},n=N+1}^{2N} \right) \varphi_{\mathbf{R}n} |\mathbf{R}n\rangle \quad (1)$$

Here  $n = 1, \dots, N$  denotes the basis functions  $|\mathbf{R}n\rangle$  of the top layer and  $n = N + 1, \dots, 2N$  denotes the basis functions of the bottom layer. These basis functions are usually required to be sufficiently localized in real space in order to minimize the overlap matrix elements that are truncated in tight-binding calculations. In this study, we use  $N = 22$  spinor maximally-localized Wannier functions (MLWFs) [10] as basis functions

for each MoS<sub>2</sub> monolayer primitive unit cell. These MLWFs are a set of orthogonal functions constructed using linear combinations of Bloch functions from density functional theory (DFT) calculation. The total real-space spread of these functions is minimized through an iterative minimization scheme.

To generate the desired MLWFs, non-collinear DFT calculations on a MoS<sub>2</sub> monolayer were first performed using OpenMX [11]. The local spin density approximation of Ceperley-Alder (LSDA-CA) [12] is used for the exchange-correlation functional within these intra-layer calculations. The kinetic energy cutoff and k-mesh size are set to be 200 Ryd and 12×12×1 respectively. The MoS<sub>2</sub> monolayer structure is constructed using experimental data  $a = 3.160$  Å and  $c = 3.172$  Å [13], with which the band gap can be nicely reproduced [14]. The band gap we calculated is about  $E_g = 1.8$  eV, in accordance with the results in [14].

Previous DFT studies [15,16] show that the energy bands of a MoS<sub>2</sub> monolayer near the band gap are formed primarily from the Mo-4d and S-3p orbitals. We thus use these 22 orbitals including spin up and down as trial orbitals and choose an inner energy window between  $-7$  eV and  $5$  eV for the construction of 22 MLWFs for each primitive unit cell. Ten of these MLWFs are centered about the Mo atoms and retain the d-orbital features, and six are centered about each of the two S atoms and retain the p-orbital features (Fig. 2(a)). The total spread, defined as  $\sum_{n=1}^{22} (\langle r^2 \rangle_n - \langle \mathbf{r} \rangle_n^2)$ , of these MLWFs is about  $35$  Å<sup>2</sup>, which means that on average each MLWF is well localized near its center with an expected radius about  $1.26$  Å. The overlap matrix elements between these MLWFs up to the 3rd nearest cells are also calculated. Fig. 2(b) shows the band structure calculated using these MLWFs and overlap matrix elements as the tight-binding basis set and hopping potentials, respectively, as compared to the original DFT calculations. The band structure is accurately reproduced in the energy range within our interest by using these MLWFs as tight-binding basis functions.

### C. Calculation formalism for the exchange-coupled bilayer

With a total of 44 MLWFs in each *two-layer* unit cell, we write for the tight-binding wave-function,

$$\boldsymbol{\varphi}_{\mathbf{R}} = (\varphi_{\mathbf{R},1}, \dots, \varphi_{\mathbf{R},N}; \varphi_{\mathbf{R},N+1}, \dots, \varphi_{\mathbf{R},2N})^T = \begin{pmatrix} \boldsymbol{\varphi}_{\mathbf{R},\text{T}} \\ \boldsymbol{\varphi}_{\mathbf{R},\text{B}} \end{pmatrix} \quad (2)$$

in (1). The Schrödinger equation then is

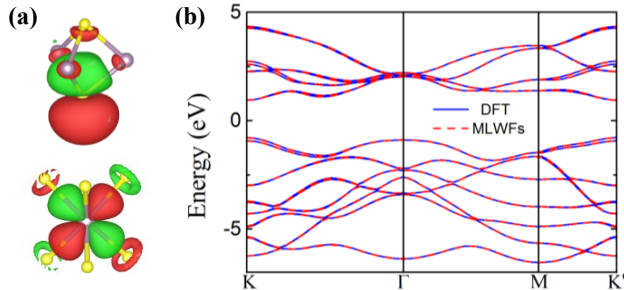


Fig. 2. (a) Isosurface plots of an S-centered  $p_z$ -like MLWF (top) and a Mo-centered  $d_{z^2}$ -like MLWF (bottom), plotted with VESTA [17]. Positive values are in red and negative values are in green. Only the real part is plotted. The imaginary part is small compared to the real part. (b) Comparison of the band structure obtained from DFT calculations with that calculated using a tight-binding basis of MLWFs. The Fermi level serves as the zero energy reference. The temperature is 300 K.

$$\sum_{\mathbf{R}'} \mathbf{H}_{\mathbf{R}\mathbf{R}'} \boldsymbol{\varphi}_{\mathbf{R}'}^{(\beta)} = E^{(\beta)} \boldsymbol{\varphi}_{\mathbf{R}}^{(\beta)} \quad (3)$$

where  $\beta = \{\mathbf{k}, \alpha\}$  represents a single electron state with wave-vector  $\mathbf{k}$  and band index  $\alpha$ . Here we have assumed the in-plane scale of the two layers to be large enough to apply Bloch theorem which gives  $\boldsymbol{\varphi}_{\mathbf{R}}^{(\mathbf{k}, \alpha)} = e^{i\mathbf{k} \cdot \mathbf{R}} \boldsymbol{\varphi}_{\mathbf{0}}^{(\mathbf{k}, \alpha)}$ , where  $\mathbf{0}$  labels the lattice site at origin, so that (3) can be reduced to a secular equation for  $\boldsymbol{\varphi}_{\mathbf{0}}^{(\beta)}$  and associated energy  $E^{(\beta)}$ .

As for the graphene system in [18], the Hamiltonian of (3) takes the form,

$$\mathbf{H}_{\mathbf{R}\mathbf{R}'} = \begin{bmatrix} \mathbf{H}_{\mathbf{R},\text{T};\mathbf{R}',\text{T}} - qV_{\text{T}}\mathbf{I} & \mathbf{H}_{\mathbf{R},\text{T};\mathbf{R}',\text{B}} \\ \mathbf{H}_{\mathbf{R},\text{B};\mathbf{R}',\text{T}} & \mathbf{H}_{\mathbf{R},\text{B};\mathbf{R}',\text{B}} - qV_{\text{B}}\mathbf{I} \end{bmatrix} \quad (4)$$

Here,  $\mathbf{H}_{\mathbf{R},\text{T};\mathbf{R}',\text{T}}$  and  $\mathbf{H}_{\mathbf{R},\text{B};\mathbf{R}',\text{B}}$  are the *intra-layer* tight-binding Hamiltonian of each MoS<sub>2</sub> monolayer obtained from the DFT calculations as described in Section II.B;  $\mathbf{I}$  is the identity matrix and  $q$  is the magnitude of the electron charge. The local Hartree potential and any variations in the *intra-layer* exchange-correlation potential with carrier concentration are described by local electrostatic-like potentials of top layer ( $V_{\text{T}}$ ) and bottom layer ( $V_{\text{B}}$ ), respectively. In our simulation, with zero interlayer bias (zero interlayer Fermi level difference), these potentials are set to create an electron concentration  $n$  in the top layer and a hole concentration  $p$  in the bottom layer. Once set,  $V_{\text{T}}$  and  $V_{\text{B}}$  remain constant in the following calculations. In practice, these potentials can be controlled by doping and/or by external gates. Exciton condensation is favored by balanced carrier concentrations,  $n = p$ . Thus,  $V_{\text{T}}$  and  $V_{\text{B}}$  are carefully chosen to achieve this condition, at least initially. No “bare” single-particle coupling potentials are considered between the layers. Instead,  $\mathbf{H}_{\mathbf{R},\text{T};\mathbf{R}',\text{B}}$  is just the *interlayer* Fock exchange interaction approximated as

$$\mathbf{H}_{\mathbf{R},\text{T};\mathbf{R}',\text{B}} = -\frac{q^2/(4\pi\epsilon_r\epsilon_0)}{|\mathbf{r}_{\mathbf{R},\text{T}} - \mathbf{r}_{\mathbf{R}',\text{B}}|} \sum_{\beta'} f(\beta') \boldsymbol{\varphi}_{\mathbf{R},\text{T}}^{(\beta')} \boldsymbol{\varphi}_{\mathbf{R}',\text{B}}^{(\beta')\dagger} \quad (5)$$

and similarly for  $\mathbf{H}_{\mathbf{R},\text{B};\mathbf{R}',\text{T}}$ , on which condensate formation rests. Here  $\mathbf{r}_{\mathbf{R},\text{T}(\text{B})}$  denotes the centers of the MLWFs on the top (bottom) layer in the unit cell labeled by  $\mathbf{R}$  and implicitly incorporates an interlayer separation  $d$  in addition to in-plane position;  $f$  is the Fermi-Dirac distribution function.

The Schrödinger equation (3) and the Fock exchange interaction (5) must be solved self-consistently. We employed an iterative method as follows: Given some small initial perturbations in the Fock interaction matrix, (3) can be solved for each state  $\beta$ . Since different states are independent in (3), they can be calculated by different computer processors. Therefore parallelized computation is readily used to reduce computation time. After all states are obtained, they are used to recalculate the Fock interaction of (5). The new Fock interaction is then used to recalculate the electron states  $\beta$ . This process is repeated until convergence is achieved.

## III. RESULTS

### A. Condensate formation

Exciton condensate formation in bilayer systems is characterized by a self-consistent delocalization of the wave-

functions  $\phi_{\mathbf{R}}^{(\beta)}$  and associated enhancement of the exchange interaction [6,18]. One measurable result of this enhancement is a band gap opening or, in this case, enhanced opening of an existing gap. Fig. 3(a) shows the simulated band structure of this bilayer system at room temperature with  $n = p = 5 \times 10^{12} \text{ cm}^{-2}$  initially, with and without the Fock interaction that mediates condensate formation. A much larger nominally interlayer band gap of about 250 meV can be seen in the presence of condensate near the band edges (K points), compared to the original band gap of about 65 meV. Fig. 3(b) illustrates the delocalization between the layers in the states  $\beta$  near the band edges at the K and K' points. The conduction band minimum has 16% contribution from the bottom, nominally hole, layer and the valence band maximum has 44% contribution from the top, nominally electron, layer. However, states far from the band edges remain strongly localized to one or the other layer, and contribute much less to the condensation, accordingly.

### B. Strength of condensate

In [18], the coherence-induced band gap size is used as a measure of the condensate strength in the bilayer graphene system. However in this MoS<sub>2</sub> system there can be a preexisting gap—or band overlap—whose size depends on the input parameters  $V_T$  and  $V_B$ . Thus this measure of the condensate strength is modified as the difference in band gaps,  $E_{g,f} - E_{g,i}$ , between the band structure with (“final state” labeled “f”) and without (“initial state” labeled “i”) condensate.

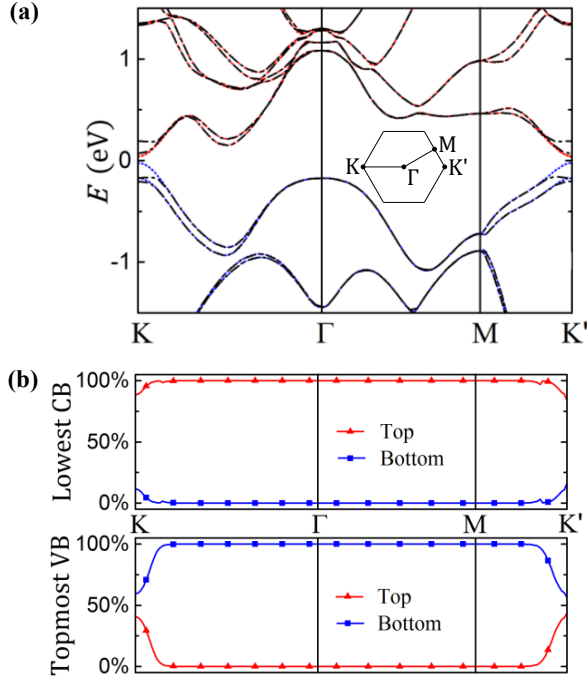


Fig. 3. (a) The band structure of the bilayer MoS<sub>2</sub> system with (black dash-dotted lines) and without (color dotted lines) Fock exchange interaction at temperature  $T = 300 \text{ K}$ . In the latter one, red and blue represent states localized to the top and the bottom layer, respectively. The other parameters are  $\epsilon_r = 3$ ,  $d = 1 \text{ nm}$ , and, initially,  $n = p = 5 \times 10^{12} \text{ cm}^{-2}$ . (b) Associated contributions of top layer and bottom layer components of the wave-functions to the lowest conduction band and topmost valence band of the Fock-exchange coupled system, showing delocalization of the wave-functions between layers near the K and K' points. (The k-space resolution is much finer than the symbol spacing.)

Fig. 4 shows the dependence of the thus-measured condensate strength on various parameters. The condensate strength attenuates with increasing interlayer separation  $d$ , and dielectric constant  $\epsilon_r$  as expected due to the weakening of the underlying interlayer Coulomb interaction. The condensate strength also attenuates and eventually collapses entirely at a “critical temperature”  $T_c$  for this condensate, much as for conventional superconductivity but, at least under the assumptions made here, at potentially much larger temperatures.

### C. Charge density dependence

Larger initial carrier concentrations also yield stronger condensates. Although they remain nearly balanced, the final charge densities in the layers are much greater than the initial carrier concentrations (Fig. 5). However, these layer charge densities are not from free carriers (electrons in the conduction band and vacancies in the valence band) of which few remain because the greatly enhanced energy gap about the Fermi level (zero eV reference). Rather, charge results from the delocalization of near-valence-band-edge states between the layers that transfers negative charge from the bottom layer to the top layer (See again Fig. 3(b)).

Although the band gap differences between initial state (without condensate) and final state (with condensate) change accordingly to initial carrier concentrations, the band gap in the presence of the condensate is a relative weak function of the charge densities as shown in Fig. 6. Even in the case when the

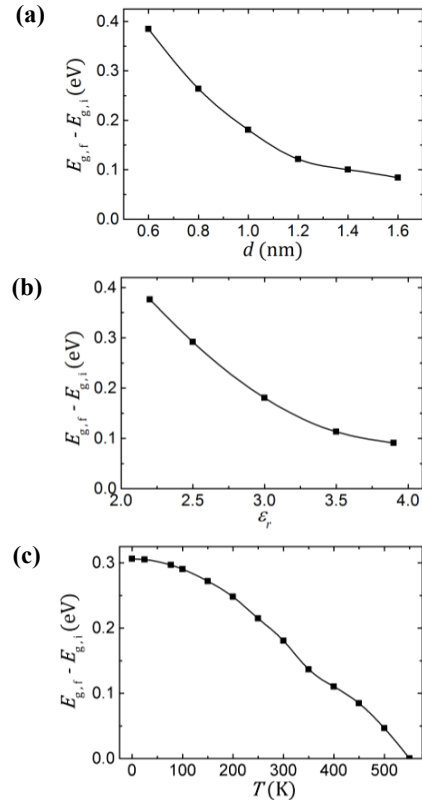


Fig. 4. The condensate strength as a function of (a) interlayer separation; (b) dielectric constant; and (c) temperature. If not an explicit variable in the figures, the parameters are  $T = 300 \text{ K}$ ,  $\epsilon_r = 3.0$ ,  $d = 1 \text{ nm}$ , and initially,  $n = p = 5 \times 10^{12} \text{ cm}^{-2}$ .

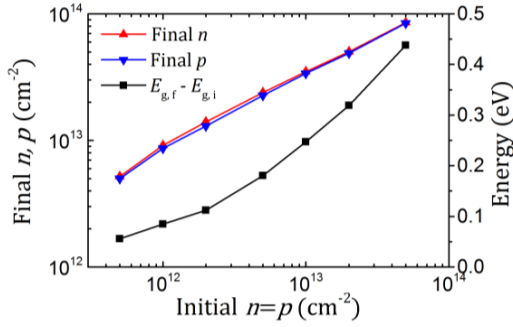


Fig. 5. Layer charge densities—associated with delocalization between layers of the near valence band-edge states—in units of the electron charge  $q$  and condensate strength, both after condensate formed as a function of equal initial charge densities. The parameters are  $d = 1$  nm,  $T = 300$  K, and  $\epsilon_r = 3$ .

initial conduction band and valence band overlap with each other, the condensate band gap still resides in a range between 250 meV and 300 meV. In other words, there is a roughly constant minimum binding energy required to ionize an exciton (create an electron hole pair), which is roughly that of an effective-mass-based calculation of a single electron-hole pair interlayer exciton binding energy [19].

#### IV. CONCLUSION

We illustrate the essential physics of exciton condensate formation between two dielectrically separated MoS<sub>2</sub> monolayers through simulations. The interlayer Fock exchange interaction that mediates condensate formation is incorporated within tight-binding simulations with an intra-layer MLWF basis set and coupling potentials derived from DFT calculations. While we can readily produce room-temperature condensates in these simulations, detailed screening and other considerations not addressed here could limit formation to lower temperatures [9]. Here we focus on qualitative physics and essential trends. Closer layer proximity, low- $\kappa$  interlayer dielectric, and higher carrier concentration will be preferable for the formation of condensate as all increase the Coulomb interaction that underlies the Fock exchange interaction. However, charge densities are enhanced by condensate formation for fixed layer potentials. In practice, this result would mean still larger associated electric fields to create the given layer potentials, or quantitatively more limited condensate formation. As noted earlier, the use of dissimilar TMD layers with staggered or broken gap band alignments could minimize the required interlayer fields. Although the material system used here is simplified, the basic method could be modified easily to model similar systems with such dissimilar TMD materials. Work is underway to extend this basic tight-binding approach to investigate transport properties through finite systems, although perhaps with simpler tight-binding models for larger systems.

#### ACKNOWLEDGMENTS

This work was supported by the Semiconductor Research Corporation Nanoelectronics Research Initiative's (SRC-NRI's) South West Academy of Nanoelectronics (SWAN) center.

#### REFERENCES

[1] J. P. Eisenstein and A. H. MacDonald, "Bose-Einstein condensation of excitons in bilayer electron systems," *Nature* **432**, 691 (2004).

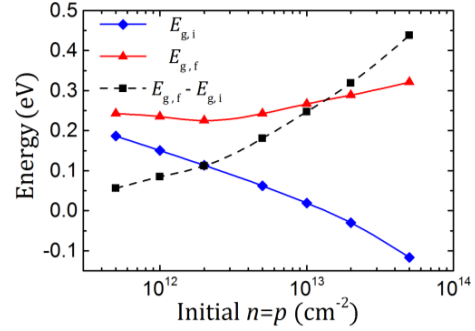


Fig. 6. Initial and the final nominally interlayer band gaps, as measured from the band edges. A negative initial band gap indicates the overlap of the conduction band of one layer and valence band of the other. The simulation parameters are  $d = 1$  nm,  $T = 300$  K, and  $\epsilon_r = 3$ .

- [2] D. Nandi, A. D. K. Finck, J. P. Eisenstein, L. N. Pfeiffer, and K. W. West, "Exciton condensation and perfect Coulomb drag," *Nature* **488**, 481 (2012).
- [3] J.-J. Su and A. H. MacDonald, "How to make a bilayer exciton condensate flow," *Nature Phys.* **4**, 799 (2008).
- [4] X. Mou, L. F. Register, and S. K. Banerjee, "Quantum transport simulations on the feasibility of the bilayer pseudospin field effect transistor (BiSFET)," *International Electron Devices Meeting (IEDM)* 4.7.1 (2013).
- [5] S. K. Banerjee, L. F. Register, E. Tutuc, D. Reddy, and A. H. MacDonald, "Bilayer pseudospin field-effect transistor (BiSFET): a proposed new logic device," *IEEE Elec. Dev. Lett.* **30**, 158 (2009).
- [6] H. Min, R. Bistritzer, J.-J. Su, and A. H. MacDonald, "Room-temperature superfluidity in graphene bilayers," *Phys. Rev. B* **78**, 121401 (2008).
- [7] I. Sodemann, D. A. Pesin, and A. H. MacDonald, "Interaction-enhanced coherence between two-dimensional Dirac layers," *Phys. Rev. B* **85**, 195136 (2012).
- [8] Communication with A. H. MacDonald.
- [9] F.-C. Wu, F. Xue, and A. H. MacDonald, "Theory of spatially indirect equilibrium exciton condensates," arXiv:1506.01947, submitted for publication (2015).
- [10] N. Marzari, A. A. Mostofi, J. R. Yates, I. Souza, and D. Vanderbilt, "Maximally localized Wannier functions: Theory and applications," *Rev. Mod. Phys.* **84**, 1419 (2012).
- [11] T. Ozaki, OpenMX, <http://www.openmx-square.org/>.
- [12] D. M. Ceperley and B. J. Alder, "Ground state of the electron gas by a stochastic method," *Phys. Rev. Lett.* **45**, 566 (1980).
- [13] A. A. Al-Hilli and B. L. Evans, "The preparation and properties of transition metal dichalcogenide single crystals," *J. Cryst. Growth* **15**, 93 (1972).
- [14] J. Chang, L. F. Register, and S. K. Banerjee, "Ballistic performance comparison of monolayer transition metal dichalcogenide MX<sub>2</sub> (M=Mo, W; X=S, Se, Te) metal-oxide-semiconductor field effect transistors," *J. Appl. Phys.* **115**, 084506 (2014).
- [15] A. Kuc, N. Zibouche, and T. Heine, "Influence of quantum confinement on the electronic structure of the transition metal sulfide TS<sub>2</sub>," *Phys. Rev. B* **83**, 245213 (2011).
- [16] S. Lebegue and O. Eriksson, "Electronic structure of two-dimensional crystals from ab initio theory," *Phys. Rev. B* **79**, 115409 (2009).
- [17] K. Momma and F. Izumi, "VESTA 3 for three-dimensional visualization of crystal, volumetric and morphology data," *J. Appl. Cryst.* **44**, 1272 (2011).
- [18] D. Basu, L. F. Register, D. Reddy, A. H. MacDonald, and S. K. Banerjee, "Tight-binding study of electron-hole pair condensation in graphene bilayers: Gate control and system-parameter dependence," *Phys. Rev. B* **82**, 075409 (2010).
- [19] D. Reddy, L. F. Register, and S. K. Banerjee, unpublished.